Int. J. Electrochem. Sci., 16 **(2021)** Article ID: 210460, doi: 10.20964/2021.04.19

International Journal of
ELECTROCHEMICAL
SCIENCE
www.electrochemsci.org

Addition of $LuCl_3$ for Improving Micro-structure and Corrosion Resistance of Micro-arc Oxidation Coating Formed on 6061

Dan Xiong[1], *Ping Wang*[1,2,*], *Xiao Wei Shen*[1], *Ji Wei Liu*[1], *Biao Yang*[1], *Yun Bai Gong*[1], *Ze Yu Gong*[1], *Jie Hu*[1], *Dong Xiang*[1]

[1] School of New Energy and Materials, Southwest Petroleum University, Chengdu, 610500, China
[2] School of Physics, University of Electronic Science and Technology of China, Chengdu, 611731, China
Corresponding author: Wang Ping, Ph.D., Professor, School of Materials Science and Engineering, Southwest Petroleum University, Chengdu, 610500, China, P. R. China, Tel: 028-83037405,
[*]E-mail: 818wp@163.com

Received: 8 December 2020 / *Accepted:* 19 January 2021 / *Published:* 28 February 2021

$LuCl_3$ was added to an electrolyte to prepare micro-arc oxidation coatings on 6061 aluminium alloys. The influence of $LuCl_3$ on the micro-structure and properties of the MAO coating was studied by Scanning Electron Microscope, Energy Dispersive Spectrometer, X-ray Diffraction and electrochemical workstation. Results showed that the addition of $LuCl_3$ caused a change in the oxidation voltage, which affected the micro-structure and performance of the coating. The micro-arc oxide coating containing $LuCl_3$ was mainly composed of γ-Al_2O_3 and SiO_2. $LuCl_3$ entered the coating in the form of $LuCl_3$ and $Lu_2(C_2O_4)$•H_2O. The micro-arc oxidation coating formed in the electrolyte containing $LuCl_3$ was denser, smoother and less porous, with higher hardness and better corrosion resistance than the coating without $LuCl_3$. Therefore, the addition of $LuCl_3$ into the electrolyte could change the oxidation process of the micro-arc oxide coating, thus improving the micro-structure and corrosion resistance of the coating.

Keywords: Micro-arc oxidation; $LuCl_3$ particles; 6061 aluminum alloy; Structure; Corrosion resistance

1. INTRODUCTION

Because of its advantages of high specific strength, low density and easy processing, 6061 aluminium alloy is widely used in automobile manufacturing [1-2]. However, its relatively poor hardness, corrosion resistance and wear resistance affect its further development [3-4]. Many researchers have focused on improving the properties of aluminium alloys through surface modification techniques, such as laser cladding [5], electroplating [6], chemical vapor deposition

(CVD) [7], and thermal spraying [8]. However, these technologies have the disadvantages of high pollution, high cost and harsh conditions.

Micro-arc oxidation is an environmentally friendly surface treatment technology that can effectively improve the performance of aluminium alloys [9-11]. The quality of micro-arc oxidation coatings is influenced by electrolyte composition [12], substrate [13] and electrical parameters [14-15]. At present, the influence of dopants in electrolytes on micro-arc oxidation coatings is being widely studied [16], especially rare earth compounds [17-18]. Similar to adding $Ce(SO_4)_2$ to the electrolyte, the hardness, uniformity and corrosion resistance of the coating can be improved [19]. $LuCl_3$ is a rare earth compound with wide industrial value. Adding a small amount of $LuCl_3$ in the process of smelting the alloy can refine and improve the uniformity of the grains in the alloy. The formation mechanism of the micro-arc oxidation coating is that the high temperature generated by the micro-arc discharge causes the surface of the substrate to melt and sinter to form a ceramic coating, which involves complex physical and chemical changes. In some respects, it is similar to the alloy melting process. Therefore, it is reasonable to believe that adding $LuCl_3$ into the micro-arc oxidation electrolyte promotes the formed micro-arc oxidation coating to be more uniform and denser. There have been no reports of adding $LuCl_3$ to micro-arc oxide coatings. Therefore, $LuCl_3$ was selected as an additive in this study to study the effects of $LuCl_3$ on the micro-structure and properties of a micro-arc oxide coating of 6061 aluminium alloy.

2. EXPERIMENTAL PROCEDURE

2.1. Preparation of the MAO coating

Rectangular samples of 6061 aluminium alloy (with the following chemical composition by wt%: Mg 0.8-1.2%, Si 0.40-0.80%, Cu 0.15-1.40%, Fe 0.00-0.70%, Cr 0.04-0.35%, Zn ≤ 0.25%, Mn ≤ 0.15%, Ti ≤ 0.15% and Al balance) were used as substrate materials in the experiments. The specimens, with dimensions of 10×10×3 mm, were polished and degreased before the MAO process. The base electrolyte consisted of 10 $g \cdot L^{-1}$ Na_2SiO_3, 0.7 $g \cdot L^{-1}$ $(NaPO_3)_6$, 0.1 $g \cdot L^{-1}$ NaOH, 1 $g \cdot L^{-1}$ NaF and 3 $ml \cdot L^{-1}$ $C_3H_8O_3$. Before MAO treatment, the surface of the samples was polished by silicon carbide papers with grit number sizes between 400 and 2000. The substrate was then cleaned with deionized water and dried in ambient air. Two groups of samples were prepared for comparison. One group of samples was prepared in an electrolyte containing no $LuCl_3$, while the other group was prepared in an electrolyte containing 0.08 $g \cdot L^{-1}$ $LuCl_3$, which had the greatest influence on the properties of the micro-arc oxide coating, especially in improving its corrosion resistance. In addition, the electrolyte was continuously stirred during the treatment to maintain uniformity. The MAO coatings were fabricated at a peak current density of 3 $A \cdot dm^{-2}$ for 20 min, a fixed frequency of 100 Hz and a duty cycle of 50%. This process was carried out using pulsed electrical power that provided a positive pulse voltage. The temperature of the electrolyte was kept below 30°C by a heat-exchange system during the MAO process. After MAO treatment, the specimens were rinsed with hot water at 95°C for 5 min and then dried in air.

2.2. Coating analysis

The conductivity of each electrolyte was measured ten times to take the average value with a digital conductivity meter (DDS-11A, YOKE Instrument, China). The surface and cross-sectional morphologies of the MAO coatings were observed by Scanning Electron Microscopy (SEM, ZEISS EVO MA15, Carl Zeiss Microscopy GmbH, Germany) equipped with the ability to perform Energy Dispersive Spectroscopy (EDS, OXFORD 20, Carl Zeiss Microscopy GmbH, Germany), which can detect the elemental content and distribution. The phase composition of the coatings was investigated by X-ray diffraction (XRD, DX-2700B, HAOYUAN Instrument, China) with a Cu Kα radiation source (λ= 1.5418 Å). Diffraction data were acquired in grazing incidence mode (grazing angle of 3°) with a 2θ range from 10 to 80° (scanning speed of 0.05°/s) at 40 kV and 30 mA. The target elements were detected by X-ray photoelectron spectroscopy (XPS, ESCALAB 250X, Thermo Scientific, America). Furthermore, the adhesion between the substrate and coatings was evaluated by a multifunctional surface performance tester (MFT-4000, Lanzhou Huahui Instrument Technology, China) with automatic loading from 0 to 20 N at a loading rate of 10 $N \cdot min^{-1}$. In addition, thermal shock tests of the coatings were investigated by using an electric chamber furnace (SX-10-12, Beijing Dexi Technology, China), which was heated to 500°C for 10 min and then cooled down to 25°C water for 50 cycles. The micro-hardness of the coatings was measured ten times for each specimen to take the average value with a digital micro-hardness tester (HVS-1000, Haoxinda Instrument, China) at 1 N for 15 s. The surface roughness of the coating was measured by a surface roughness meter (HD350, Zhongtong Hengchuang Testing Technology, China), each sample was measured ten times, and the average value was taken. An Electrochemical Workstation (Reference 3000, Gamry, America) was used to acquire polarization curves and electrochemical impedance spectroscopy in a 3.5% NaCl solution at room temperature. Before each test, the sample was placed in the 3.5% NaCl solution for a period of time to allow the working electrode to reach the steady state.

3. RESULTS AND DISCUSSION

3.1. Conductivity of electrolyte

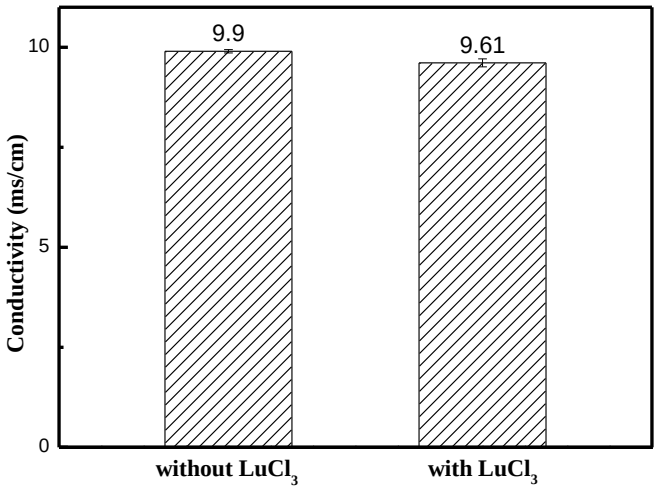

Figure 1. Electrical conductivity of used electrolyte in the presence and the absence of $LuCl_3$.

Figure 1 shows the conductivity of the electrolyte with and without $LuCl_3$. Figure 1 shows that after adding 0.08 g/L $LuCl_3$, the conductivity of the electrolyte decreases from 9.9 mS/cm to 9.61 mS/cm. Although the electrolyte with $LuCl_3$ shows a lower conductivity, a conductive path is formed on the coating surface, which enhances the transfer of static charges [20]. Therefore, the sample prepared in the electrolyte containing $LuCl_3$ has a lower voltage during the first and second stages under constant current conditions, as shown in stages I and II in Figure 2.

3.2. Voltage-time response during MAO process

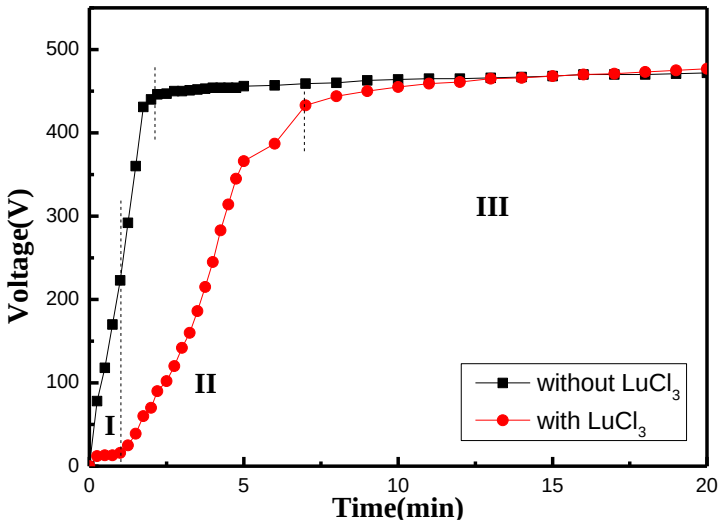

Figure 2. Voltage-time curves of the samples during MAO treatment at constant current density (3 $A \cdot dm^{-2}$) in used electrolyte in the presence and the absence of $LuCl_3$.

To investigate the effects that the addition of $LuCl_3$ to the electrolyte has on the nature of the micro-structure during the MAO process, changes in the response voltage with increasing oxidation time were evaluated. Figure 2 shows the responding voltage-time curves of the samples treated in electrolytes with and without $LuCl_3$ during the MAO process. As shown in Figure 2, the microarc oxidation process is divided into three stages: anodization, spark anodization, and micro-arc oxidation [21]. In stage I, the anodizing stage (0 to 2 min), the responding voltage rapidly and linearly increases due to the formation and growth of an insulation layer [22]. In stage II, in the spark anodizing stage (2 to 4 min with the solution without $LuCl_3$ and 2 to 7 min with the solution with $LuCl_3$), the voltage further increases to reach the critical value, leading to the breakdown of weak parts on the substrate surface. In stage III, in the micro-arc oxidation stage (4/7 to 20 min), the voltage tends to be stable, and the substrate is continuously broken down and immediately covered by molten material; thus, the coating is continuously thickened. It can be clearly seen from Figure 2 that compared to that with the electrolyte without $LuCl_3$, the voltage increases more slowly during the first stage of the micro-arc oxidation process with the electrolyte with $LuCl_3$. This result is because under the action of an electric field, $LuCl_3$ are adsorbed on the surface of the sample, making the insulating layer thicker and suppressing the increase in voltage. However, compared with the electrolyte not containing $LuCl_3$, the

time needed for the second stage of micro-arc oxidation with the electrolyte containing $LuCl_3$ increases significantly, and the breakdown voltage value decreases. This result is because the addition of $LuCl_3$ enhances the conductivity of the electrolyte, and the increase in conductivity reduces the voltage value. However, due to the absorption of $LuCl_3$ on the surface of the substrate, the breakdown of the substrate is more difficult and takes more time. In the third stage of micro-arc oxidation, the voltage basically remains unchanged; that is, the addition of $LuCl_3$ has little influence on the third stage of micro-arc oxidation. The third stage of micro-arc oxidation is the period where the coating thickness increases rapidly. This is also why the coating thickness does not change significantly before and after the addition of particles, as shown in Figure 3.

3.3. Micro-structure of the coatings

3.3.1. Morphology and EDS analyses of the coatings

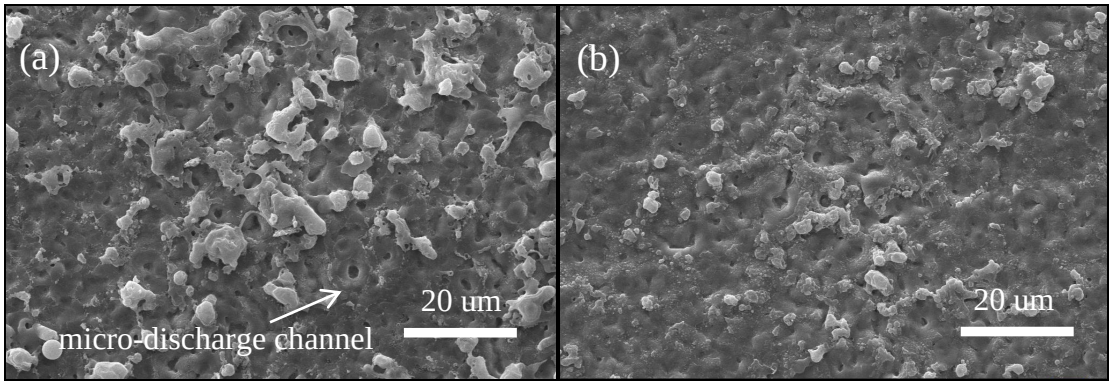

Figure 3. Surface morphology of MAO coatings prepared in used electrolyte in the presence and the absence of $LuCl_3$: (a) without $LuCl_3$ and (b) with $LuCl_3$.

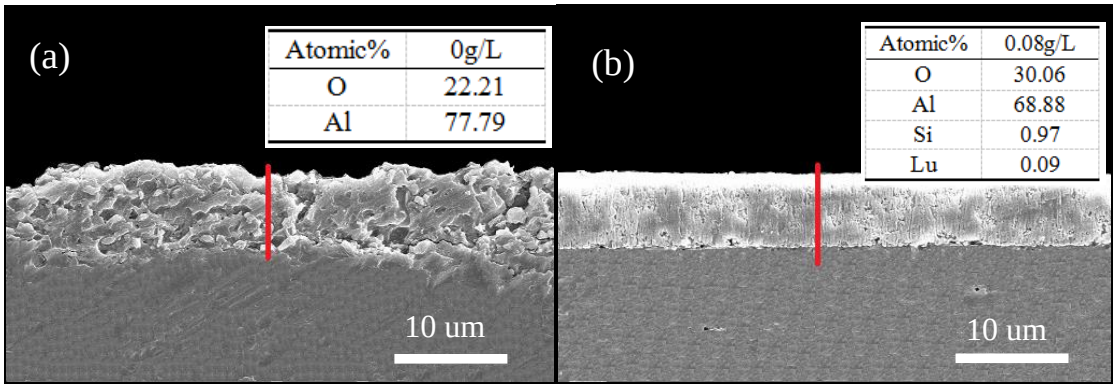

Figure 4. The cross-sectional morphology of the MAO coatings prepared in used electrolyte in the presence and the absence of $LuCl_3$ and its line scan element atomic percentage: (a) without $LuCl_3$ and (b) with $LuCl_3$.

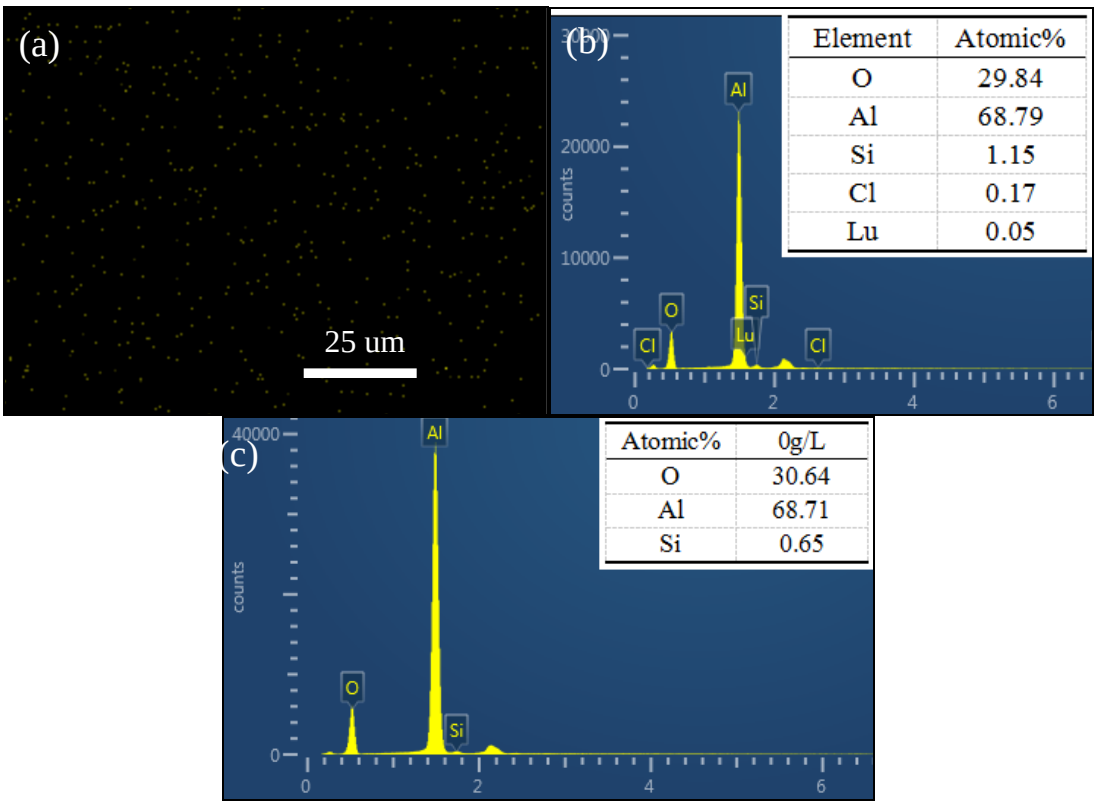

Figure 5. Surface element analysis of MAO coatings prepared in used electrolyte in the presence and the absence of $LuCl_3$: (a) distribution of Lu elements on the surface of the MAO coating prepared in electrolyte containing $LuCl_3$, (b) surface element analysis of MAO coating prepared in electrolyte containing $LuCl_3$, and (c) surface element analysis of MAO coating prepared in electrolyte without $LuCl_3$.

Figure 3 shows the surface morphology of the MAO coatings formed in an electrolyte with and without $LuCl_3$. The MAO layer exhibits a typical crater-like morphology resulting from the local micro-discharge during coating formation in the MAO stage, as shown in Figure 3 (a). This structure is caused by molten material flowing out of the micro-discharge channel during the spark process. The molten material diffuses on the surface, collides with the electrolyte and solidifies rapidly [23]. Figure 3 shows that the addition of $LuCl_3$ has a large effect on the surface morphology. The surface of the sample formed in the solution without $LuCl_3$ is coarser and clearly has a porous structure. However, the surface morphology of samples formed in the solution with $LuCl_3$ has relatively low roughness and porosity. This result is consistent with the roughness situation reflected in Figure 9. Moreover, the sample containing $LuCl_3$ is smoother and attracts some small particles. This is consistent with the cross-sectional morphology shown in Figure 4. Compared with the coatings formed in the solution without $LuCl_3$, the coatings formed in the solution with $LuCl_3$ are denser and more uniform. In addition, the discharge channel of the coating with $LuCl_3$ is sealed better. This is because the addition of $LuCl_3$ will increase the discharge centre and balance the discharge energy, resulting in grain refinement. In addition, at the high temperature and pressure of micro-arc oxidation, $LuCl_3$ melts into the discharge channel, which is blocked by the cooled particles, making the surface smooth and reducing the number of discharge holes, as shown in Figure 3 (a) and Figure 3 (b). This result is also

why the breakdown of the sample formed in the solution containing $LuCl_3$ is more difficult and takes longer, as shown in Figure 1. The thickness of the coating formed in the solution without $LuCl_3$ is approximately 8 μm, which is approximately the same as the coating thickness prepared in the solution with $LuCl_3$. This result is consistent with the situation reflected by the oxidation voltage. As shown in Figure 1, in the process of preparing the coating, the voltages of the two samples are basically the same during the third stage of micro-arc oxidation, which determines the coating thickness. Therefore, the coating thickness prepared in the electrolyte containing $LuCl_3$ is basically the same as that prepared in the electrolyte without $LuCl_3$.

Figure 5 shows a diagram of Energy Dispersive Spectroscopy results of the sample. Figure 5 (a) shows the distribution of Lu on the surface of the coating made in the solution with $LuCl_3$. Figure 5 (b) shows the surface element content diagram of the coating containing $LuCl_3$, and Figure 5 (c) shows the surface element content diagram of the coating without $LuCl_3$. The results show that Lu successfully enters the coating and is evenly distributed on the surface of the coating. EDS elemental composition analysis results of the sample section also shows that $LuCl_3$ successfully enter the micro-arc oxidation coating and participate in the formation of the coating despite the content of $LuCl_3$ being relatively low. This indicates that the changes in the surface micro-structure of the coating are indeed caused by $LuCl_3$ under the same experimental conditions. From the cross-sectional elemental content of the sample in Figure 4 (a) and (b) and the surface elemental content in Figure 5 (b) and (c), it can be seen that the Si content of the coating containing $LuCl_3$ is much greater than that of the coating without $LuCl_3$. This result is because the surface of the coating containing $LuCl_3$ is smoother and has almost no discharge channels. The surface of the coating without $LuCl_3$ is uneven, and the discharge channel is obvious. During the EDS test, only the element signals on the upper surface of the sample can be received, while the element signals on the lower surface and in the holes of the sample are almost absent. Compared with other elements, the content of Si is lower, which is consistent with the XRD results. Therefore, the more holes there are on the sample surface, the more difficult it is to detect the Si signal. This result is why the coating containing $LuCl_3$ has a higher Si content than the coating without $LuCl_3$.

3.3.2. Phase analysis of the coatings

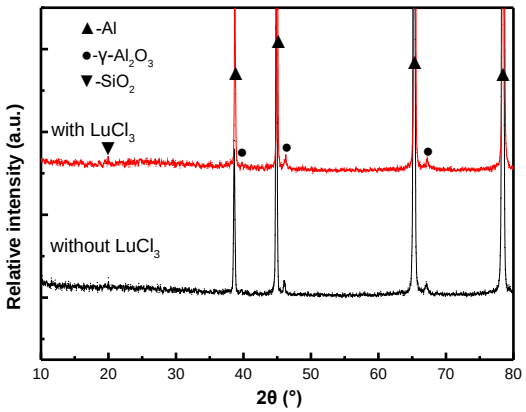

Figure 6. X-ray diffraction patterns of micro-arc oxidation coatings prepared in used electrolyte in the presence and the absence of $LuCl_3$.

To verify the effect of adding $LuCl_3$ to each phase in the MAO coating, XRD analysis was used to determine the phase composition, as shown in Figure 6. The results show that the prepared MAO coating is mainly composed of Al, SiO_2 and γ-Al_2O_3. Figure 6 shows that the XRD patterns of the coating prepared with and without $LuCl_3$ in the electrolyte are almost the same. This result shows that the addition of $LuCl_3$ in the electrolyte has almost no effect on the phase composition of the micro-arc oxidation coating. Therefore, $LuCl_3$ improves the performance of the coating by changing the formation process of the coating rather than changing the phase composition of the coating. The 6061 Al substrate exhibits corresponding peaks in all diffraction patterns because X-rays penetrate the coating and hit the substrate [24]. Both SiO_2 and γ-Al_2O_3 are produced by oxidation during micro-arc discharge. Generally, at a certain temperature, γ-Al_2O_3 will be converted to α-Al_2O_3 or both phases will exist together. The transformation relation between γ-Al_2O_3 and α-Al_2O_3 is:

$$\gamma\text{-}Al_2O_3 \xrightarrow{\text{More than } 1223\,\text{k}} \alpha\text{-}Al_2O_3 \quad (1)$$

As shown in Figure 6, the microarc oxidation coating contains only γ-Al_2O_3 and no α-Al_2O_3. This result may be because the α-Al_2O_3 content is too low to be detected. This observation may also be because in the process of micro-arc oxidation, the surface temperature of the substrate is too low to support the conversion from γ-Al_2O_3 to α-Al_2O_3. According to the energy consumption of micro-arc oxidation:

$$E = W/Sd \quad (2)$$

where W is the energy consumption of micro-arc oxidation (kWh), S is the micro-arc oxidation area (m^2), d is the film thickness (m), and E is the unit energy consumption (kWh/ m^2·m). The 1 μm coating formed on the surface of the aluminium alloy consumes approximately 0.1 kwh /m^2. Thus, in this experiment, the energy consumption is:

$$W = ESd = 0.1kWh/m^2 \cdot \mu m \times 3.2\times10^{-4} m^2 \times 8\mu m = 2.56\times10^{-4} kWh \quad (3)$$

$$Q = W \times 3599712J/kWh = 921.5J \quad (4)$$

During micro-arc oxidation, most of the energy is lost in the form of heat, with only 15%-45% of the energy used for the oxidation and phase transition of the coating. Therefore, only 138.2-414.7 J of heat is applied to the coating. Thus, the maximum instantaneous discharge temperature on the sample surface is only 865.6 K according to $dQ = cmdT$. This result is lower than the transition temperature from γ-Al_2O_3 to α-Al_2O_3. Therefore, only γ-Al_2O_3 is detected in the coating.

$LuCl_3$ does not exist because the amount of $LuCl_3$ added is too small to be detected by XRD. However, EDS shows that both Lu and Cl successfully enter the coating. To further verify the presence of $LuCl_3$ in the coating, XPS detection was performed.

3.3.3. XPS analyses of the coatings

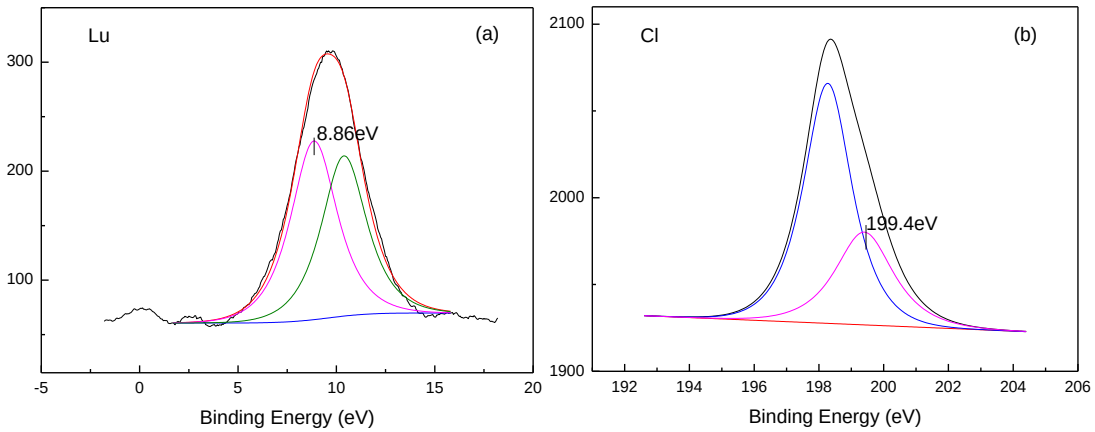

Figure 7. XPS survey scan of core level spectra of Lu 4f and Cl 2p of MAO coating prepared in electrolyte containing 0.08 g/L $LuCl_3$.

The elemental valence and surface chemical composition of the samples were investigated by XPS. Figure 7 shows the energy spectra of Lu and Cl in the sample manufactured in the solution containing 0.08 g/L $LuCl_3$. Lu and Cl mainly exist in the coating with $Lu_2(C_2O_4)_3$▪H_2O (Lu 4f: 8.86 eV) and $LuCl_3$ (Cl 2p: 199.4 eV).

In combination with the EDS, XRD and XPS results, the MAO technique for coating growth on the 6061 aluminium alloy surface may include the following processes:

$$Al + O_2 \xrightarrow{\text{oxidation}} Al_2O_3 \xrightarrow{micro-arc} \gamma - Al_2O_3 \quad (5)$$

$$2LuCl_3 + 6CO_2 + H_2O \xrightarrow{micro-arc} Lu_2(C_2O_4)_3 \bullet H_2O + 3Cl_2 \uparrow \quad (6)$$

$$LuCl_3(particle) \xrightarrow{hydrolyze} LuCl_3 \bullet 6H_2O(electrolyte) \xrightarrow{micro-arc} LuCl_3(coating) \quad (7)$$

Therefore, $LuCl_3$ enters the coating in two forms: $Lu_2(C_2O_4)$•H_2O and $LuCl_3$. In the process of micro-arc oxidation, some $LuCl_3$ react with H_2O in the electrolyte, and CO_2 dissolves in the electrolyte to form $Lu_2(C_2O_4)$•H_2O; CO_2 comes from the air in the open system. The other portion of $LuCl_3$ absorb water in the electrolyte to form $LuCl_3$•$6H_2O$, which is dehydrated at the high temperature and pressure of micro-arc oxidation. Finally, this portion of $LuCl_3$ is embedded in a molten coating in the form of particles, which contacts the cold electrolyte and quickly cools to form a coating. It is in these two ways that $LuCl_3$ successfully enter the coating. XRD shows that there is no $Lu_2(C_2O_4)$•H_2O or $LuCl_3$ in the coating, which indicates that few particles enter the coating in the above two forms. Therefore, $LuCl_3$ in the electrolyte has a larger effect on the discharge process of the coating, thereby affecting the coating formation process rather than changing the phase composition of the coating.

3.4. Analysis of the coating properties

3.4.1. Micro-hardness and adhesive strength of the coatings

The changes in the average adhesive strength and micro-hardness of the specimens coated in

electrolytes with and without $LuCl_3$ are shown in Figure 8. After the addition of $LuCl_3$, the micro-hardness of the coating increases, while the change in adhesive strength decreases. Studies have shown that the adhesion between the coating and the substrate is positively correlated with the thickness of the coating. However, the thickness of the coating is determined by the voltage in the micro-arc oxidation stage. As shown in Figure 2, although the addition of $LuCl_3$ causes the action time of the micro-arc oxidation stage to become shorter, its intensity remains unchanged. Therefore, there is no obvious change in the thickness of the coating, but the adhesive strength between the coating and the substrate slightly decreases, as shown in Figure 8. This insignificant decrease may be due to the different zigzag bonds between the coating and substrate. As shown in Figure 4, compared with the coating containing $LuCl_3$, the zigzag bond between the coating without $LuCl_3$ and the substrate is more obvious, which is why the adhesive strength is slightly higher [25]. The hardness of micro-arc oxidation-treated samples is much higher than that of the substrate, which is due to the hard γ-Al_2O_3 phase produced after micro-arc oxidation. The hardness of the coating increases after the addition of $LuCl_3$. The reason is that the addition of $LuCl_3$ leads to grain refinement and solid solution strengthening.

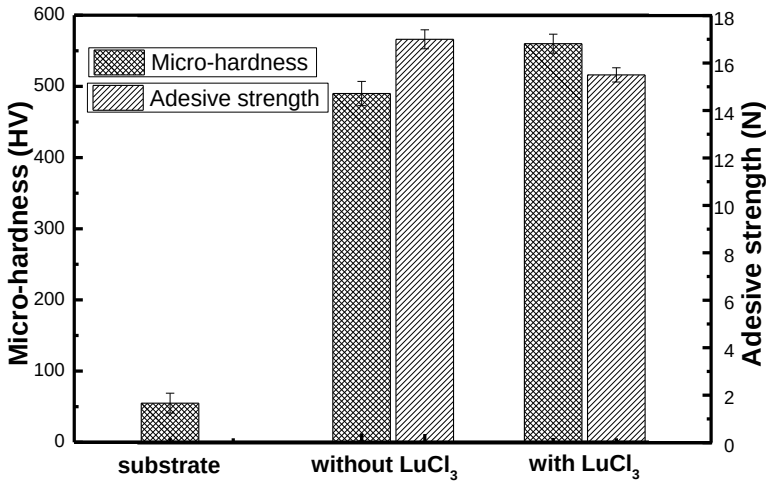

Figure 8. The hardness of the substrate and the hardness, adhesive strength of the MAO coatings prepared in used electrolyte in the presence and the absence of $LuCl_3$.

3.4.2. Surface roughness of the coating

Figure 9 shows the surface roughness of the coating prepared in the electrolyte with and without $LuCl_3$. Figure 9 shows that the surface of the coating prepared in the electrolyte containing $LuCl_3$ is smoother. This result is consistent with the situation reflected in Figure 3. The surface roughness of the sample decreases from 0.996 μm to 0.6542 μm after the addition of $LuCl_3$ to the electrolyte. This observation proves that the addition of $LuCl_3$ in the electrolyte can indeed decrease the surface roughness of the MAO coating, and this change is caused by the decrease in the number of micropores [26]. By changing the formation process of the micro-arc oxidation coating, the particles

block the discharge channels on the surface of the sample, and the coating becomes smoother and denser.

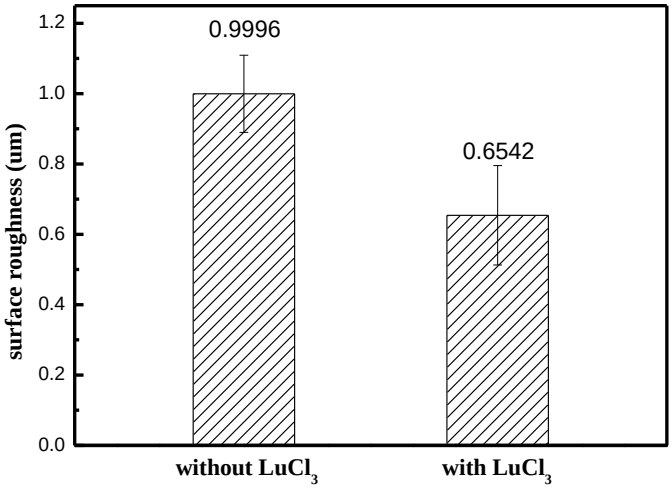

Figure 9. Surface roughness of MAO coatings prepared in used electrolyte in the presence and the absence of $LuCl_3$.

3.4.3. Thermal shock test of the MAO coatings

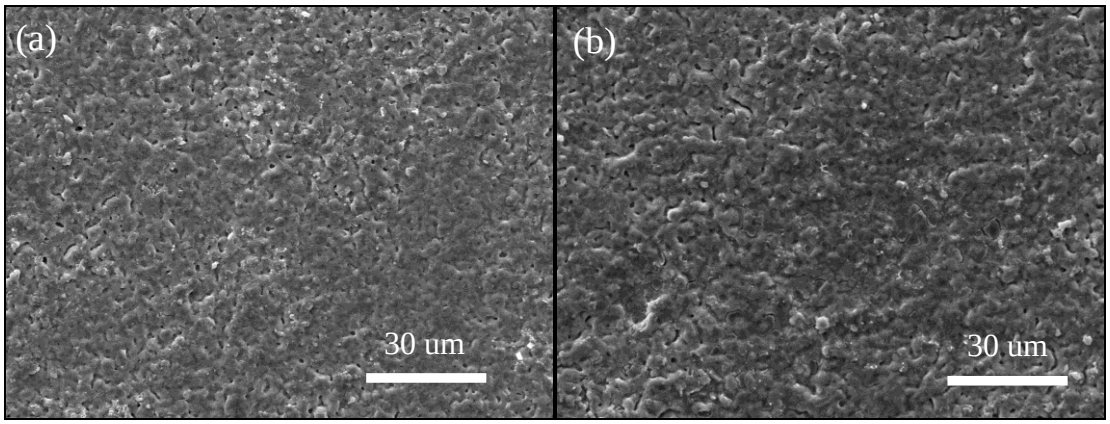

Figure 10. Surface morphology of MAO coatings prepared in used electrolyte in the presence and the absence of $LuCl_3$ after the thermal shock tests: (a) without $LuCl_3$ and (b) with $LuCl_3$.

The surface morphology of each coating after the thermal shock test is shown in Figure 10. Figure 10 (a) shows the surface morphology of the sample without $LuCl_3$, while Figure 10 (b) shows the surface morphology of the sample containing $LuCl_3$. The thermal shock test involves heating the sample to 500°C, keeping it at that temperature for 10 min, and then cooling it in 25°C deionized water for 50 cycles. In the repeated thermal expansion and contraction process, the coating will be detached from the substrate due to thermal stress, especially in the case of low adhesion [27]. The coating

containing $LuCl_3$ is denser and more prone to cracking due to stress concentration. However, there was no obvious peeling or cracking between the coating and substrate (as shown in Figure 10). This result is because the coating is well bonded to the substrate. Furthermore, this observation indicates that the addition of $LuCl_3$ does not reduce the thermal shock resistance of the coating when the other properties of the coating are improved.

3.5. Corrosion resistance of the MAO coatings

3.5.1. Potentiodynamic polarization

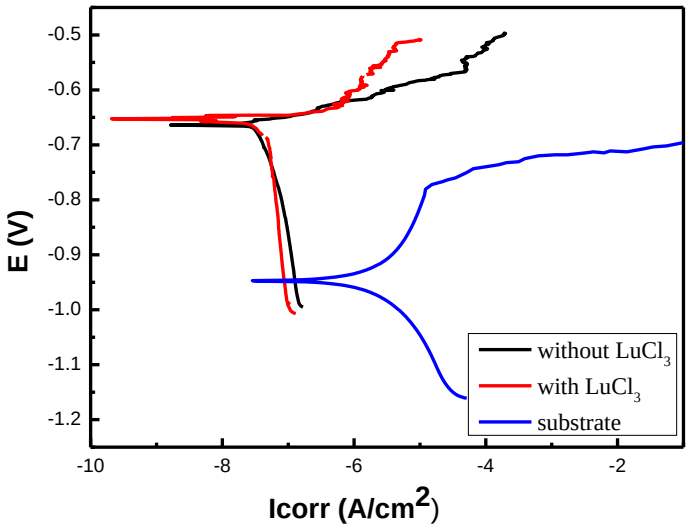

Figure 11. Polarization curves of the substrate and the MAO coatings prepared in used electrolyte in the presence and the absence of $LuCl_3$.

Table 1. Potentiodynamic polarization data for the MAO coatings prepared in used electrolyte in the presence and the absence of $LuCl_3$

Sample	E_{corr}(V)	I_{corr}(A·cm^{-2})	Corrosion rate (mpy)
Substrate	-0.9475	4.06×10^{-6}	0.9625
Without $LuCl_3$	-0.6640	4.39×10^{-8}	3.050×10^{-2}
With $LuCl_3$	-0.5720	2.840×10^{-8}	1.298×10^{-2}

The polarization curve of the oxidation film in a 3.5% NaCl aqueous solution is presented in Figure 11. Table 1 shows the results of the polarization curves obtained by Tafel fitting, including the corrosion current density, corrosion potential and corrosion rate. It is obvious that when $LuCl_3$ is added to the electrolyte, the polarization curves shift to the left and upward, which means a lower corrosion current density and higher corrosion potential. In general, a high corrosion potential and low corrosion

current density suggest good corrosion resistance [28]. This result means that in a 3.5 wt.% NaCl solution, the corrosion resistance of the sample prepared in the solution containing $LuCl_3$ is higher than that of the sample prepared in the solution without $LuCl_3$. This result can also be seen in Table 1, where the corrosion rate of the sample prepared in the solution containing $LuCl_3$ is lower than that of the sample prepared in the solution without $LuCl_3$. Furthermore, the ceramic-coated samples have higher corrosion potential and corrosion current density than the uncoated aluminium alloys. Clearly, the corrosion resistance of the sample after the micro-arc oxidation treatment is far greater than that of the aluminium substrate. This result is because the micro-arc oxidation coating can prevent chloride ions from contacting and corroding the substrate. However, the coating formed without adding $LuCl_3$ to the electrolyte has obvious discharge channels, as shown in Figure 3 (a). These channels can cause Cl^- to penetrate the coating and corrode the substrate. Adding $LuCl_3$ to the electrolyte greatly reduces this possibility. In the micro-arc oxidation process, $LuCl_3$ affect the discharge process of the micro-arc oxidation coating, thereby affecting the formation of the coating, causing the discharge channel of the coating to be blocked by some particles; thus, the coating becomes denser. The dense coating effectively prevents the corrosion of Cl^- on the substrate, thereby improving the corrosion resistance of the coating. This result also shows that the presence of $LuCl_3$ significantly improves the overall corrosion resistance of the coating.

3.5.2. Electrochemical impedance spectroscopy

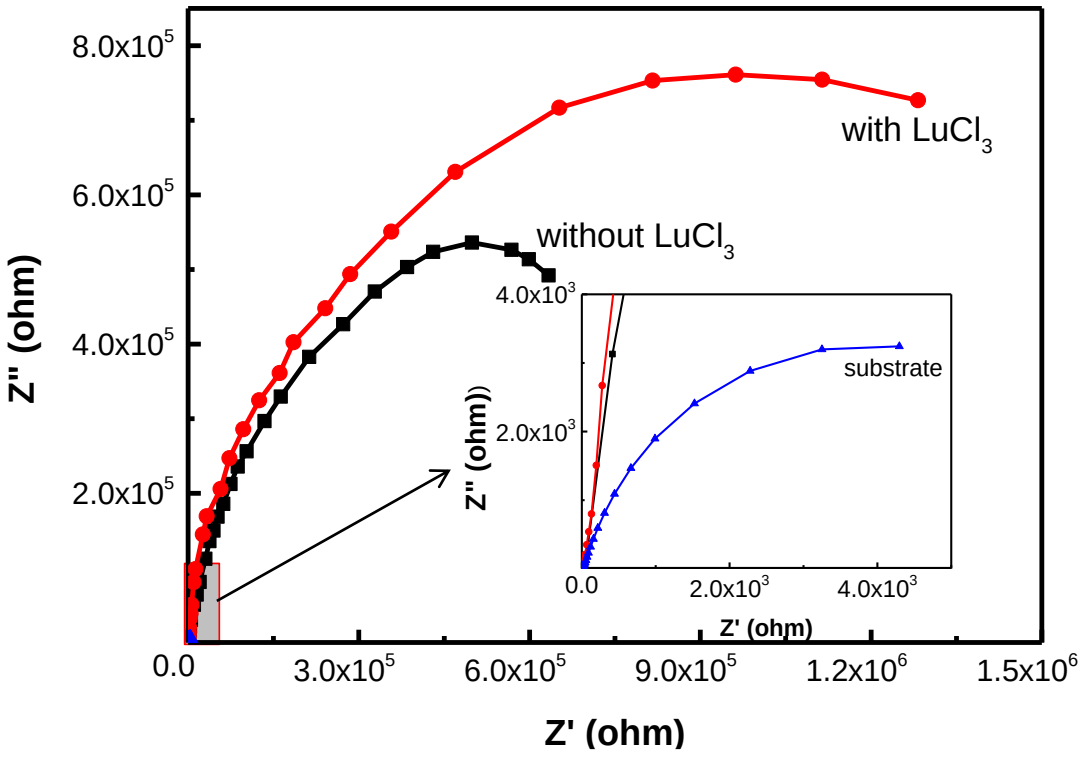

Figure 12. Nyquist plots for the MAO coatings formed in used electrolyte in the presence and the absence of $LuCl_3$.

To further understand the corrosion behaviour of coatings, EIS tests were conducted. Figure 12 exhibits the Nyquist plots for the MAO coatings formed in both the $LuCl_3$ and $LuCl_3$-free electrolytes. Due to the charge transfer process, the MAO coatings are characterized by a capacitive loop [29]. The radius of the capacitive loop of the coating containing $LuCl_3$ is significantly larger than the radius of the capacitive loop of the coating not containing $LuCl_3$, indicating that that the former has better corrosion resistance, as shown in Figure 12. Clearly, the corrosion resistance of the sample after micro-arc oxidation treatment is much greater than that of the 6061 aluminium substrate. This result is consistent with the polarization curve. The corrosion resistance is determined by the thickness and compactness of the coating. The thicker and tighter the coating is, the less easy it is for Cl^- to enter the coating and corrode the substrate. From the surface morphology of the coating, it can be seen that the coating formed in the solution with $LuCl_3$ is more compact, so it is natural that it has better corrosion resistance.

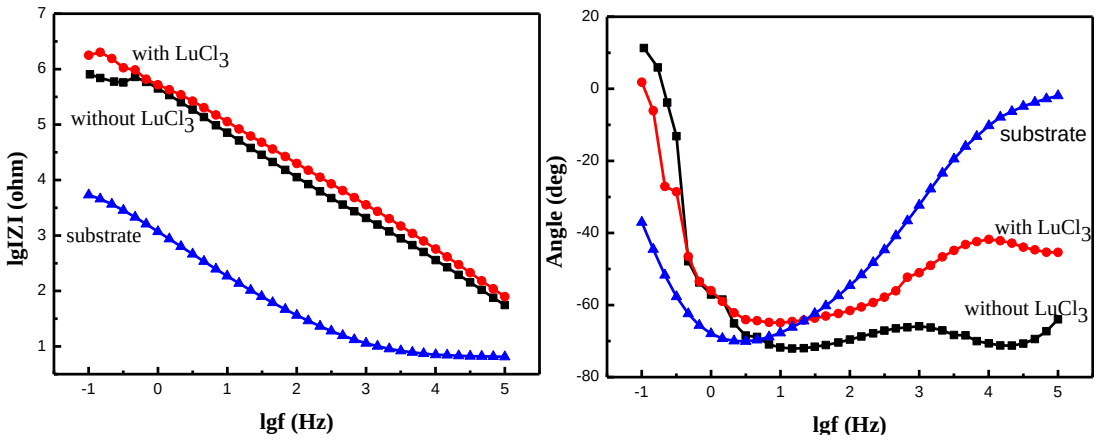

Figure 13. EIS Bode plots of the MAO coatings formed in used electrolyte in the presence and the absence of $LuCl_3$: (a) impedance modulus; (b) phase angle.

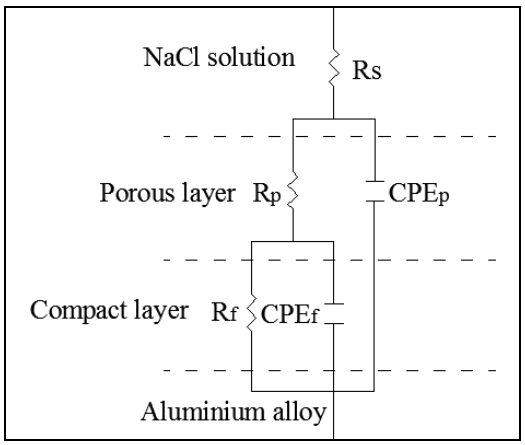

Figure 14. Electrochemical equivalent circuit of the MAO coatings prepared in used electrolyte in the presence and the absence of $LuCl_3$.

Table 2. Electrochemical parameters of substrate and MAO coatings prepared in used electrolyte in the presence and the absence of $LuCl_3$ obtained via the equivalent circuit fitting of the EIS results.

Sample	R_S (Ω▪cm^2)	CPE_P(f▪cm^2)		R_P (Ω▪cm^2)	CPE_f(f▪cm^2)		R_f (Ω▪cm^2)
		Y_0 (S▪sec^n)	n		Y_0 (S▪sec^n)	n	
Substrate	6.882	2.023×10^{-4}	0.7708	1.213×10^{4}	-	-	-
Without $LuCl_3$	11.34	3.351×10^{-7}	0.7769	7.382×10^{3}	1.43×10^{-7}	0.8	1.034×10^{6}
With $LuCl_3$	7.01	2.52×10^{-8}	0.8416	2.32×10^{7}	8.828×10^{-10}	0.8636	1.46×10^{6}

Figure 13 shows the EIS Bode plots of specimens treated in the solution with and without $LuCl_3$. When the coating is divided into an outer loose layer and an inner dense layer and the solution penetrates the coating and contacts the substrate, there are three capacitive time constants. When the solution permeates the coating and does not touch the substrate, there are two capacitive time constants, which represents the information of the outer porous and inner barrier layers of the coating, respectively. When the substrate is directly corroded, there is only one capacitive time constant. In Figure 3, there is no clear dividing line between the inner and outer layers of both coating (b) and coating (a). However, it can be clearly seen from Figure 13 that the EIS behaviour of the specimens after micro-arc oxidation has two capacitance time constants, representing the inner and outer layers. Therefore, the electrochemical equivalent circuit shown in Figure 14 is adopted for fitting. The fitting curves and test curves are basically identical, indicating that the equivalent circuit model is properly designed. In this equivalent circuit, Rs is the solution resistance, while R_P and P_f represent the resistance of the porous layer and compact layer, respectively, and are connected in parallel with the constant phase elements CPE_P and CPE_f [30]. The electrochemical parameters of each sample were obtained by equivalent circuit fitting of the electrochemical impedance spectroscopy results, as shown in Table 2. As seen from Table 2, the resistance Rs of the solution does not change much, and the resistance R_f of the inner layer of the coating is generally larger than the resistance R_P of the outer layer, which proves that the inner layer plays a crucial role in the corrosion resistance of the sample. Compared with the samples prepared in the solution with and without $LuCl_3$, the n value of the samples prepared in the solution with $LuCl_3$ is greater than that in the solution without $LuCl_3$, while the Y_0 value is smaller, indicating that the samples containing $LuCl_3$ are denser, with a lower roughness and better corrosion resistance. The low-frequency resistance R in Bode plots can be used to evaluate the corrosion resistance of micro-arc oxidation coating samples [31]. As shown in Figure 13, the R of samples containing $LuCl_3$ in the coating is significantly higher than that of samples without $LuCl_3$ in the coating. Therefore, the corrosion resistance of the samples containing $LuCl_3$ in the coating is higher than that of the samples without $LuCl_3$ in the coating. This observation is consistent with the above results. In general, all the results show that the coating containing $LuCl_3$ has better corrosion resistance, which proves that $LuCl_3$ is conducive to improving the corrosion resistance of the MAO coating.

4. CONCLUSIONS

The effect of the addition of $LuCl_3$ on the micro-structure and properties of a 6061 aluminium alloy micro-arc oxide coating was studied. The addition of $LuCl_3$ caused a change in the oxidation voltage and extended the time for the voltage to reach the breakdown voltage. As a result, the coating became smoother and denser, and the number and size of micropores decreased. Some properties of the coating also changed. The adhesion between the coating and the substrate decreased slightly, from 17 N to 15.5 N, but the thermal shock resistance did not. The coating was composed of Al, SiO_2 and γ-Al_2O_3. $LuCl_3$ successfully participated in the formation process of the coating, promoting grain refinement and solid solution strengthening and increasing the hardness of the coating from 490 HV to 560 HV. The corrosion resistance of the coating was also improved (increasing by approximately 2×10^{-2} mpy) with an increasing coating density. Therefore, the addition of $LuCl_3$ in the electrolyte could effectively improve the micro-structure and performance of micro-arc oxidation coatings, especially corrosion resistance.

ACKNOWLEDGEMENTS
This work was supported by China Postdoctoral Science Foundation (2019M663470).

References

1. M.A. Chen, Y.C. Ou, Y.H. Fu, Z.H. Li, J.M. Li and S.D. Liu, *Surf. Coat. Technol.*, 304 (2016) 85.
2. P. Wang, T. Wu, Y.T. Xiao, J. Pu, X.Y. Guo, J. Huang and C.L. Xiang, *J. Mater. Eng. Perform.*, 25 (2016) 9.
3. W.M. Xia, N. Li and B. Deng, *Ceram. Int*., 45 (2019) 8.
4. Z.W. Li and S.C. Di, *J. Mater. Eng. Perform*., 26 (2017) 4.
5. Y.L. Fu, N. Guo, C. Zhou, G.H. Wang, J.C. Feng, *J. Mater. Process. Technol.*, 289 (2021) 116949.
6. M. Ueda, T. Teshima, H. Matsushima and T. Ohtsuka, *J. Solid State Electrochem.*, 19 (2015)12.
7. A. Reina, X.T. Jia, J. Ho, D. Nezich, H. Son, V. Bulovic, M.S. Dresselhaus and J. Kong, *Nano Lett.*, 9 (2009) 1.
8. A. Abbas, S. Mohsen and K. Akira, *Mater. Sci. Eng., A*, 478 (2008) 1-2.
9. W.B. Dai, C.Y. Lia, D. He, D.W. Jia, Y.M. Zhang and Z. Tan, *Surf. Coat. Technol.*, 360 (2019) 347.
10. L.R. Krishna, Y. Madhavi, T. Sahithi, D.S. Rao, V.S. Ijeri, O. Prakash and S.P. Gaydos, *Fatigue Fract. Eng. Mater. Struct.*, 42 (2019) 3.
11. J. Wang, S.A. Huang, H.J. Huang, M.Y. He, P.H. Wangyang and L. Gu, *J. Alloys Compd.*, 777 (2019) 86.
12. Z.J. Wang, L.N. Wu, W. Cai, A. Shan and Z.H. Jiang, *J. Alloys Compd.*, 505 (2010) 1.
13. K.J. Wei, L. Chen and Y. Qu, Surf. Eng., 35 (2019) 8.
14. L.J. Zhu, Z.X. Guo, Y.F. Zhang, Z.X. Li and M.L. Sui, *Electrochim. Acta*, 208 (2016) 296.
15. A. Sobolev, A. Kossenko and K. Borodianskiy, *Mater.*, 12(2019) 23.
16. A. Sobolev, A. Valkov, A. Kossenko, I. Wolicki, M. Zinigrad and K. Borodianskiy, *ACS Appl. Mater. Interfaces*, 11(2019) 39534.
17. F. Liu, Y.J. Li, J.J. Gu, Q.S. Yan, Q. Luo and Q.Z. Cai, *Trans. Nonferrous Met. Soc. China*, 22(2012) 7.
18. S.Q. Wang, F.Q. Xie, X.Q. Wu and L.Y. Chen, *J. Alloys Compd.*, 788 (2019) 632.
19. P. Wang, T. Wu, Y.T. Xiao, J. Pu and X.Y. Guo, *Mater. Lett.*, 182 (2016) 27.

20. C.Y. Li, X.L. Fan, L.Y. Cui and R.C. Zeng, *Corros. Sci*., 168 (2020) 108570.
21. Y. Madhavi, L. R. Krishna and N. Narasaiah, *Int. J. Fatigue*, 126 (2019) 297.
22. P. Wang, T. Wu, Y.T. Xiao, L. Zhang, J. Pu, W.J. Cao and X.M. Zhong, *Vacuum*, 142 (2017) 21.
23. P. Wang, T. Wu, H. Peng and X.Y. Guo, *Mater. Lett.*, 170 (2016) 171.
24. A. Bordbar-Khiabani, B. Yarmand and M. Mozafari, *Surf. Coat. Technol.*, 360 (2019) 153.
25. X.W. Yang, A.B. Ma, H.A. Liu, J.H. Jiang, Y.H. Li and J.P. Sun, *Surf. Eng.*, 35 (2018) 4.
26. S.C. Di, Y.P. Guo, H.W. Lv, J. Yu and Z.W. Li, *Ceram. Int*., 41 (2015) 5.
27. P. Wang, Z.Y. Gong, J. Hu, J. Pu and W.J. Cao, *Surf. Eng.*, 35 (2019) 7.
28. D.J. Shen, G.L. Li, C.H. Guo, J. Zou, J.R. Cai, D.L. He, H.J. Ma and F.F. Liu, *Appl. Surf. Sci*., 287 (2013) 451.
29. M.Q. Tang, Z.Q. Feng, G. Li, Z.Z. Zhang and R.Z. Zhang, *Surf. Coat. Technol.*, 264 (2015) 105.
30. L.Q. Wang, J.S. Zhou, J. Liang and J.M. Chen, *Surf. Coat. Technol.*, 206 (2012) 13.
31. S.J. Xia, R. Yue, R.G. Rateick, Jr. and V.I. Birss, *J. Electrochem. Soc*., 151 (2004) 3.